Multivariate quadrature of a singular integrand

Kendall Atkinson* David Chien† Olaf Hansen‡

December 25, 2020

Abstract

Consider an integral with a point singularity in its integrand, such as $\rho^{-\alpha}$ or $\log \rho$. We introduce and discuss two methods for approximating such integrals, in both two and three dimensions. The methods are first introduced using the unit disk as the quadrature region, and then they are extended to other regions and to three dimensions. The error behavior of the numerical integration for singular points near to the boundary is examined.

Keywords: quadrature, point singularity
AMS Subject Classification: 65D32

1 Introduction

Consider calculating the singular integral

$$I(f;s) = \int_{\Omega} f(t) \log|t-s| \; dt, \qquad s \in \overline{\Omega}, \tag{1}$$

with Ω an open bounded region in the plane $\mathbb{R}^2$ and f a smooth function. This particular integral satisfies the Poisson equation

$$\Delta_s I(f;s) = -2\pi f(s), \qquad s \in \Omega.$$

The integral I is called a planar *Newtonian potential*.

With this as motivation, consider calculating the more general integral

$$I(f;s) = \int_{\Omega} f(t) k\left(|t-s|\right) \, dt, \qquad s \in \overline{\Omega}. \tag{2}$$

For example, consider

$$k\left(\rho\right) = \rho^{-\alpha}, \qquad \alpha < 2, \tag{3}$$

*University of Iowa, kendall-atkinson@uiowa.edu
†California State University San Marcos, chien@csusm.edu
‡California State University San Marcos, ohansen@csusm.edu

or

$$k(\rho) = \log \rho, \tag{4}$$

in both cases with $\rho > 0$. The problem we study is whether we can find efficient numerical methods for all $\alpha < 2$ and all $s \in \overline{\Omega}$. We first introduce some ideas for approximating such integrals over $\Omega = \mathbb{B}^2$, the unit disk. These can then be extended to more general regions Ω by using a transformation $\Phi : \mathbb{B}^2 \to \Omega$, which we illustrate in a later section. Our methods also transfer to integrands with a more general point singularity. All of our methods use a smoothing of the singularity, following it with a quadrature that benefits from the smoothing.

The numerical integration of singular functions has been studied before, and thus there also have been a number of approximation techniques proposed for their evaluation. A number of papers have been written on this topic; see, for example, [7], [10], [11], [12], and [14]. In a later section we extend our ideas to quadrature over other planar regions and over the unit ball $\mathbb{B}^3$; see §4, §5.

2 Smoothing the singularity: Method #1

We begin with the problem of approximating

$$I(g; s) = \int_{\mathbb{B}^2} g(w; s) dw, \qquad s \in \overline{\mathbb{B}}^2. \tag{5}$$

where $g(w; s)$ is allowed to be singular at $w = s$, as in (2). A procedure that has been used with univariate integrals is to make a change of the variable of integration, creating a new integrand that is smoother. For univariate integrals, see an example in [3, p.306], and an example for surface integrals is given in [4].

We look for mappings

$$\Phi_s : \mathbb{B}^2 \xrightarrow[onto]{1-1} \mathbb{B}^2 \tag{6}$$

with $\Phi_s(s) = s$ which make the singular behaviour more manageable for $w \approx s$ when using a standard quadrature over $\mathbb{B}^2$. We then calculate approximately the integral

$$I(g; s) = \int_{\mathbb{B}^2} g(\Phi_s(t); s) \left|\det D_t \Phi_s(t)\right| dt \tag{7}$$

in which we have used the transformation $w = \Phi_s(t)$, $t \in \mathbb{B}^2$. The quantity $|\det D_t \Phi_s(t)|$ denotes the Jacobian of the mapping. We want this Jacobian to decrease the singular behaviour associated around s with the integrand g in (5).

Let $s \in \overline{\mathbb{B}}^2$. Then for an arbitrary point $t \in \overline{\mathbb{B}}^2$, $t \neq s$, draw a straight line from s to t. Denote by $P_s(t)$ the point at which the continuation of that line intersects the boundary $\mathbb{S}^1 = \partial \mathbb{B}^2$; cf. Figure 1. Define

$$\Phi_s(t) = s + T\left(\frac{|t-s|^2}{|P_s(t) - s|^2}\right)(t - s), \qquad t \in \mathbb{B}^2 \backslash \{s\}. \tag{8}$$

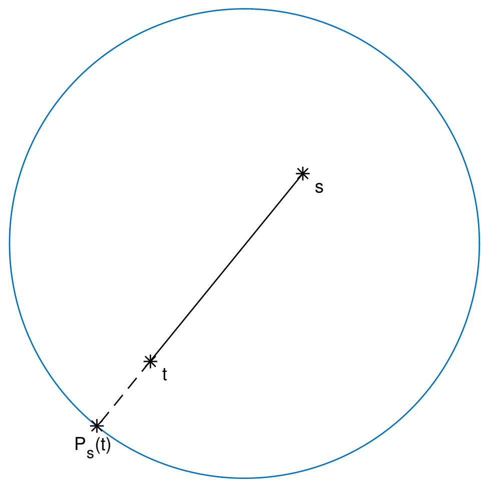

Figure 1: Illustration of $P_s\left(t\right)$

The function $T : [0,1] \to [0,1]$ is to satisfy, at a minimum,

$$\begin{aligned} &T\left(0\right) = T'\left(0\right) = 0, \\ &T\left(1\right) = 1, \\ &T'\left(r\right) > 0, \qquad 0 < r < 1. \end{aligned} \tag{9}$$

As t approaches $t_0 = P_s\left(t\right)$ on the boundary of $\mathbb{B}^2$, the fraction

$$\frac{\left|t-s\right|^2}{\left|P_s\left(t\right)-s\right|^2} \to 1,$$

and consequently, $\Phi_s\left(t\right) \to t_0$. With the above properties for $T\left(r\right)$, the mapping Φ_s of (8) satisfies (6), and moreover,

$$\Phi_s\left(s\right) = s,$$

if Φ_s is extended continuously.

As examples, we have the following.

$$T_1\left(r\right) = r^2, \tag{10}$$

$$T_2\left(r\right) = r^3, \tag{11}$$

$$T_3(r;\kappa) = \begin{cases} 0, & r = 0, \\ \exp\left(-\kappa\left(\dfrac{1-r}{r}\right)\right) & 0 < r \le 1, \end{cases} \tag{12}$$

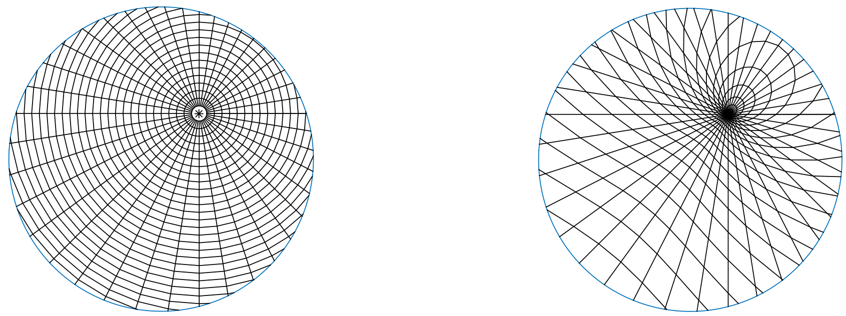

(a) Original uniform grid (b) Transformed grid

Figure 2: Illustration of mapping (8)

with $\kappa > 0$. The derivatives of the first two choices are obvious. For the third,

$$T_3'(r) = \begin{cases} 0, & r = 0, \\ \dfrac{\kappa}{r^2} \exp\left(-\kappa\left(\dfrac{1-r}{r}\right)\right), & 0 < r \leq 1, \end{cases}.$$

The main idea is to make $\det D_t \Phi_s(t)$ be zero at $t = s$, along with possibly additional derivatives. Then the integrand in (7) will be smoothed at $t = s$.

As an example of $\Phi_s(t)$ using (10), see Figure 2(b). In it, $s = (0.25, 0.3)$; and the mesh in Figure 2(b) is the transformation Φ_s applied to the mesh in Figure 2(a). Many of the circles about s in Figure 2(a) are mapped into much smaller elliptical curves about s in Figure 2(b).

2.1 Calculating the Jacobian of Φ_s

Write

$$P_s(t) = s + \sigma_+(t - s). \tag{13}$$

Using

$$1 = |P_s(t)| = |s + \sigma_+(t - s)|$$

leads to

$$|s|^2 + 2\sigma_+ s \cdot (t - s) + \sigma_+^2 |t - s|^2 = 1.$$

Solving this quadratic equation for the positive root σ_+,

$$\sigma_+ = \frac{-s \cdot (t - s) + \sqrt{[s \cdot (t - s)]^2 + \left(1 - |s|^2\right)|t - s|^2}}{|t - s|^2}$$

Note that from (13),

$$\frac{|t-s|^2}{|P_s(t)-s|^2} = \frac{1}{(\sigma_+)^2}$$

What is the Jacobian of $\Phi_s(t)$? For the components of $\Phi_s(t)$, for $j = 1, 2$, write

$$\Phi_{s,j} = s_j + T\left(\frac{1}{(\sigma_+)^2}\right)(t_j - s_j).$$

Taking the derivatives becomes complicated. To begin, for $t = (t_1, t_2)$, $j = 1, 2$, and $k = 3 - j$,

$$\begin{aligned}
\frac{\partial \Phi_{s,j}}{\partial t_j} &= T\left(\frac{1}{(\sigma_+)^2}\right) + (t_j - s_j)\, T'\left(\frac{1}{(\sigma_+)^2}\right)\frac{\partial}{\partial t_j}\left(\frac{1}{(\sigma_+)^2}\right), \\
\frac{\partial \Phi_{s,j}}{\partial t_k} &= (t_j - s_j)\, T'\left(\frac{1}{(\sigma_+)^2}\right)\frac{\partial}{\partial t_k}\left(\frac{1}{(\sigma_+)^2}\right).
\end{aligned}$$

$$\frac{\partial}{\partial t_j}\left(\frac{1}{(\sigma_+)^2}\right) = \frac{-2}{(\sigma_+)^3}\frac{\partial \sigma_+}{\partial t_j}$$

The complicated computation is to form the partial derivatives of σ_+ with respect to t_1 and t_2. For $j = 1, 2$,

$$\begin{aligned}
\frac{\partial \sigma_+}{\partial t_j} = {} & \frac{-2(t_j - s_j)}{|t-s|^4} \\
& \times \left\{ -s\cdot(t-s) + \sqrt{[s\cdot(t-s)]^2 + \left(1 - |s|^2\right)|t-s|^2} \right\} \\
& + \frac{1}{|t-s|^2}\left\{-s_j + D_j\right\}
\end{aligned}$$

$$\begin{aligned}
D_j = {} & \left\{ [s\cdot(t-s)]^2 + \left(1 - |s|^2\right)|t-s|^2 \right\}^{-\frac{1}{2}} \\
& \times \left\{ s_j\,[s\cdot(t-s)] + \left(1 - |s|^2\right)(t_j - s_j) \right\}.
\end{aligned}$$

Example 1 *In Figure 3 the Jacobian* $|\det D_t\Phi_s(t)|$ *is plotted, using* T_1 *with* $s = (0.3, 0.4)$. *It shows the Jacobian relative to the variable* t *as used in the transformed integral (7). The nodes in the* t *variable are a polar coordinates grid with 20 evenly spaced subdivisions in the radial direction and 40 subdivisions in the angular direction.*

For the numerical integration of (7), we use the well-known formula

$$\int_{\mathbb{B}^2} g(x)\, dx \approx I_n(g) \equiv \frac{2\pi}{2n+1}\sum_{l=0}^{n}\sum_{m=0}^{2n}\omega_l r_l \widehat{g}\left(r_l, \frac{2\pi\, m}{2n+1}\right) \qquad (14)$$

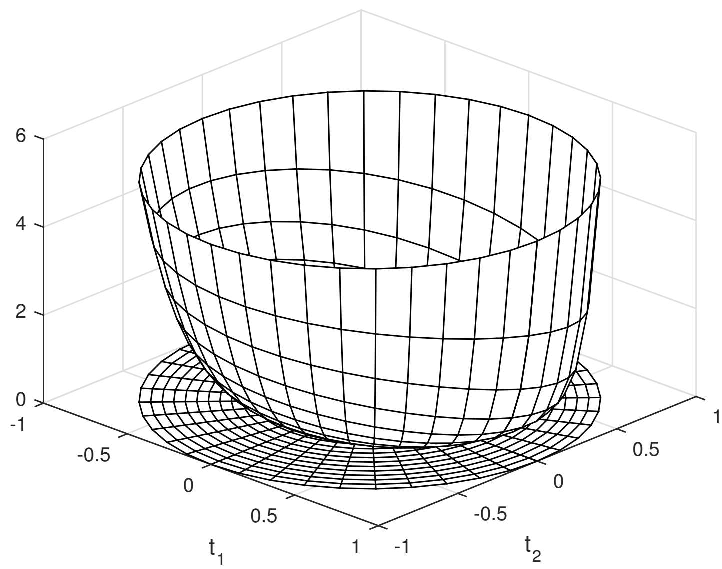

Figure 3: Jacobian of mapping (8)

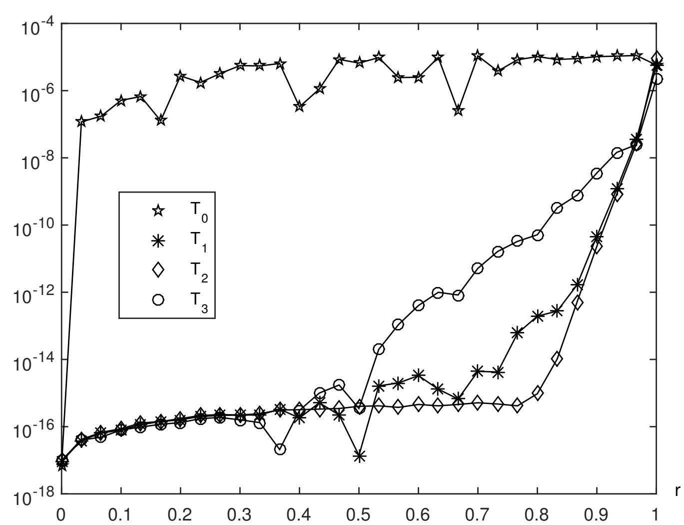

Figure 4: The quadrature error with varying T_j along the radial line $\theta = \pi/6$ using the mapping (8)

with $\widehat{g}(r,\theta) \equiv g(r\cos\theta, r\sin\theta)$. The formula uses the trapezoidal rule with $2n+1$ subdivisions for the integration over $[0,2\pi]$ in the azimuthal variable θ.The numbers r_l and ω_l are, respectively, the nodes and weights of the $(n+1)$-point Gauss-Legendre quadrature formula on $[0,1]$. This quadrature over $\mathbb{B}^2$ is exact for all polynomials $g \in \Pi_{2n}^2$; see [13, §2.6].

Example 2 *Consider the integral*

$$I(f;s) \equiv \frac{1}{2\pi}\int_{\mathbb{B}^2} f(w)\log|w-s|\,dw \qquad (15)$$
$$f(w) = J_1(\mu\rho)\cos\phi$$

with $w \equiv \rho e^{i\phi}$ *and* $\mu \doteq 2.4048255577$ *(the smallest root of* $J_0(t)$*). The true integral is*

$$I(f;s) = \lambda J_1(\mu r)\cos\theta, \quad s \equiv re^{i\theta}, \qquad (16)$$
$$\lambda = -\mu^{-2}.$$

Figure 4 shows the error in evaluating $I(f;s)$ *along the line*

$$s = r(\cos(\pi/6), \sin(\pi/6)), \qquad 0 \le r \le 1.$$

We use all three of the functions $T_j(r)$*, (10)-(12), with* $\kappa = 1$ *for* T_3*. In the graph, the case* T_0 *denotes the identity mapping* $\Phi(t) = t$*,* $t \in \mathbb{B}^2$*, meaning there is no change of variable in the integral. The integration parameter is* $n = 64$ *(the number of quadrature points is approximately* $n \times 2n$*). All three transformations work well until* $r \approx 1$*, with* T_2 *being the best. Thus there needs to be some way to improve the accuracy when* s *is near the boundary or on it, and this will also be true of our method #2.*

3 Smoothing the singularity: Method #2

In setting up another way to smooth the singularity, it is easiest to begin with the singularity in the form $s = (s_1, 0)$, $0 \le s_1 \le 1$. A rotation of the disk extends the method to more general $s \in \mathbb{B}^2$; see §3.4. Consider evaluating $I(g;s)$ using a polar coordinates representation with center at s, and initially assume $s_1 < 1$:

$$I(g;s) = \int_0^{2\pi}\int_0^{R(\theta)} g(s_1 + r\cos\theta, r\sin\theta)\, r\, dr\, d\theta, \qquad (17)$$

$$R(\theta) = -s_1\cos\theta + \sqrt{1 - s_1^2\sin^2\theta}. \qquad (18)$$

As before we are particularly interested in singularities similar to (3), (4). Introduce the mapping

$$r = T_\theta(\nu) = T\left(\frac{\nu}{R(\theta)}\right)R(\theta), \qquad 0 \le \nu \le R(\theta).$$

with the mapping T satisfying (9). Note that

$$T_{\theta}^{'}\left(\nu\right) = T^{'}\left(\frac{\nu}{R(\theta)}\right).$$

The integral becomes

$$I\left(g;s\right) = \int_{0}^{2\pi}\int_{0}^{R(\theta)} g\left(s_1 + T_{\theta}\left(\nu\right)\cos\theta, T_{\theta}\left(\nu\right)\sin\theta\right) T_{\theta}\left(\nu\right) T_{\theta}^{'}\left(\nu\right)\, d\nu\, d\theta. \tag{19}$$

For the case of $s_1 = 1$, the outer integral will be over $\left[-\frac{\pi}{2}, \frac{\pi}{2}\right]$, with

$$\begin{aligned} I(g;s) &= \int_{-\frac{\pi}{2}}^{\frac{\pi}{2}}\int_{0}^{R(\theta)} g(1 - r\cos\theta, r\sin\theta) r\, dr\, d\theta, \\ R(\theta) &= 2\cos\theta. \end{aligned} \tag{20}$$

In the case of (2)-(4), this leads to

$$I(f;s) = \int_{-\frac{\pi}{2}}^{\frac{\pi}{2}}\int_{0}^{R(\theta)} f\left(1 - r\cos\theta, r\sin\theta\right) rk\left(r\right)\, dr\, d\theta, \tag{21}$$

$$rk\left(r\right) = r\log r \quad \text{or} \quad rk\left(r\right) = r^{1-\alpha}. \tag{22}$$

3.1 Quadrature

With $0 \leq s_1 < 1$, consider using a quadrature rule on $[0, 1]$ with nodes $\{\rho_1, \ldots, \rho_n\}$ and weights $\{\omega_1, \ldots, \omega_n\}$. For the inner integral over $0 \leq \nu \leq R(\theta)$, use nodes $\{R(\theta)\rho_1, \ldots, R(\theta)\rho_n\}$ and weights $\{R(\theta)\omega_1, \ldots, R(\theta)\omega_n\}$. We use the Gauss-Legendre nodes and weights over $[0, 1]$. Apply this quadrature to the inner integral in (19):

$$\begin{aligned} &\int_{0}^{R(\theta)} g(s_1 + T_{\theta}(\nu)\cos\theta, T_{\theta}(\nu)\sin\theta)T_{\theta}(\nu)T_{\theta}'(\nu)\, d\nu \\ &\approx \sum_{j=1}^{n} R(\theta)\omega_j g(s_1 + T_{\theta}(R(\theta)\rho_j)\cos\theta, T_{\theta}(R(\theta)\rho_j)\sin\theta) \\ &\qquad \times T_{\theta}(R(\theta)\rho_j)T_{\theta}'(R(\theta)\rho_j) \end{aligned} \tag{23}$$

For the various quantities in this numerical integral,

$$\begin{aligned} T_{\theta}(R(\theta)\rho_j) &= T(\rho_j)R(\theta), \\ T_{\theta}'R(\theta)\rho_j) &= T'(\rho_j). \end{aligned} \tag{24}$$

For the angular integration over $[0, 2\pi]$, use the trapezoidal rule with $2n$ subdivisions. The total number of nodes is $n \times 2n$.

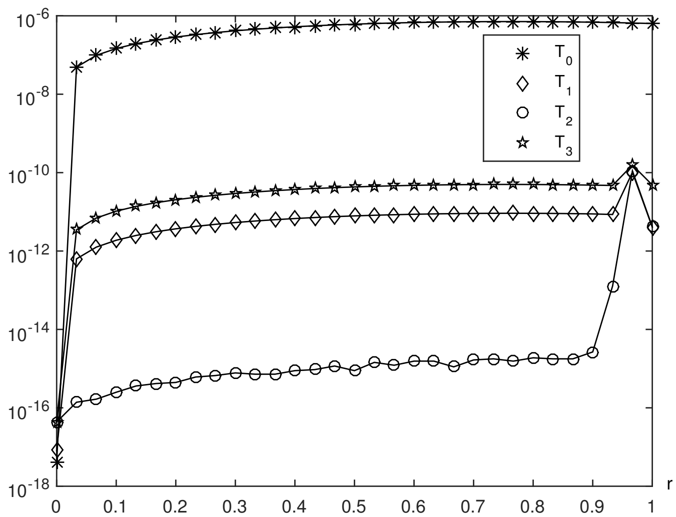

Figure 5: The quadrature error with varying T_j along the radial line $\theta = \pi/6$ using the integrals (19) and (20).

Example 3 *Evaluate the integral (15). Figure 5 shows the error in evaluating* $I(g;s)$ *along the line* $s = r(\cos(\pi/6), \sin(\pi/6))$, $0 \le r \le 1$. *We use all three of the functions* $T_j(r)$, *(10)-(12), with* $\kappa = 1$ *for* T_3. *For the boundary point* $s = (1,0)$, *we use the formulation (20), and we use* $4n$ *nodes for the* θ-*integration. In the graph, the case* T_0 *denotes the identity mapping* $T_0(r) = r$, *meaning there is no change of variable in the integral over* $0 \le r \le R(\theta)$. *(Note: This is not the same as using the identity mapping* $\Phi(t) \equiv t$ *on* $\mathbb{B}^2$ *when constructing the approximate quadrature.) The integration parameter* $n = 32$, *and the total number of nodes is* 32×64 *(until* $r = 1$ *when it is* 32×128*). Three transformations,* T_1-T_3, *work well until* $r \approx 1$. *Thus there needs to be some way to improve the accuracy when s is near the boundary or on it. This is discussed further in §3.2 and §3.6.*

Example 4 *In Figures 6(a) and 6(b), we show the integral* (15) *and error over the entire disk* $\mathbb{B}^2$. *The transformation* T_2 *is used over the interior of* $\mathbb{B}^2$, *and (20) is used for boundary calculations. The integration parameter is* $n = 16$*; and the grid uses* 15 *subdivisions in the radial direction and* 30 *in the angular direction.*

Example 5 *Evaluate the integral*

$$I(f;s) = \int_{\mathbb{B}^2} \frac{f(t)}{|t-s|^{\alpha}} dt \tag{25}$$

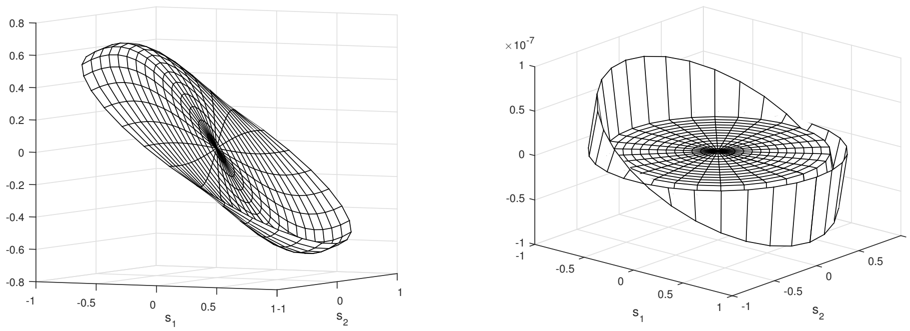

(a) The function (15)-(16).   (b) The error in evaluating (15)-(16).

Figure 6: Integration of (15)-(16).

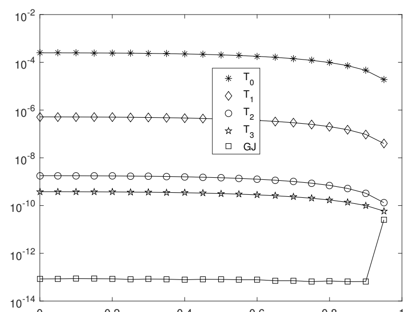

Figure 7: Quadrature of errors

with $\alpha = \pi/3$ *and*

$$f(t) = \cos(\pi t_1 t_2) - t_2^2. \tag{26}$$

The errors in the integral along the line $\theta = \pi/6$ *are shown in Figure 7. These errors are shown for the transformations* T_0, T_1, T_2, T_3, *with* $\kappa = 1$ *for* T_3. *We also use Gauss-Jacobi quadrature as discussed in the following.*

Remark. Recalling the integration (17) when applied to (24),

$$\begin{aligned} I(g;s) &= \int_0^{2\pi}\int_0^{R(\theta)} g(s_1 + r\cos\theta, r\sin\theta)\, r\; dr\, d\theta, \\ &= \int_0^{2\pi}\int_0^{R(\theta)} r^{1-\alpha} f(s_1 + r\cos\theta, r\sin\theta)\; dr\, d\theta, \end{aligned}$$

with a smooth function f. Following [8], use Gauss-Jacobi quadrature on the interval $[0, R(\theta)]$ with the weight function $r^{1-\alpha}$. If the integrand has this type of singularity (as with some of our examples), then the Gauss-Jacobi quadrature is excellent, often obtaining a small error when using a relatively small number of quadrature nodes. This is illustrated in Figure 7 of Example 5. However, if the integrand becomes more complicated, then our method with the transformation $r = T_\theta(\nu)$ is needed, as the next example demonstrates.

Example 6 *Consider the integral*

$$I(f; s) = \int_{\mathbb{B}^2} \frac{\log|t-s|}{|t-s|^\alpha} f(t)\, dt \tag{28}$$

with $\alpha = \pi/3$ and f as in (26). We evaluate the integral as in the previous example, but along the line $\theta = 0$. The numerical errors are shown in Figure 8. With the weight function $r^{1-\alpha}$, the Gauss-Jacobi method is not an improvement.

Remark. Another example for which our transformation-based methods are needed is

$$I(f; s) = \int_{\mathbb{B}^2} \frac{f(t)}{|t-s|^\alpha + |t-s|^\beta}\, dt$$

with $0 < \alpha < \beta < 2$, $\beta - \alpha \neq 1$. Examples 5 and 6 and the example in this remark indicate that the Gauss-Jacobi method is very efficient in dealing with weight singularities for which the Gauss-Jacobi weights and nodes are known. But if the weights and nodes for a Gauss-Jacobi function have to be derived first, for example for the case in Example 6, the transformation method presented in this paper seems more flexible because a fixed quadrature method is used in combination with an easily adjusted transformation. The transformation also does not need to fit the singularity perfectly, examples show that while $T_2(r) = r^3$ might be the optimal transformation, the transformation r^4 still produces very good results too.

3.2 Quadrature near the boundary.

With the integration of (20) for $s = (1, 0)$, the trapezoidal rule is no longer suitable for the angular integration. Instead we use Gauss-Legendre quadrature for $-\frac{1}{2}\pi \leq \theta \leq \frac{1}{2}\pi$, with $4n$ nodes, an empirically chosen value to improve accuracy at a boundary point. For the r-integration, motivated by (22), we proceed as before in (23). The total number of nodes is $n \times 4n$.

An alternative to handling the boundary point $s = (1, 0)$ begins with an alternative to (20):

$$\begin{aligned} I(g; s) &= \int_0^2 r \int_{-\beta(r)}^{\beta(r)} g(1 - r\cos\theta, r\sin\theta)\ d\theta\, dr, \\ \beta(r) &= \cos^{-1}\left(\tfrac{1}{2}r\right). \end{aligned} \tag{27}$$

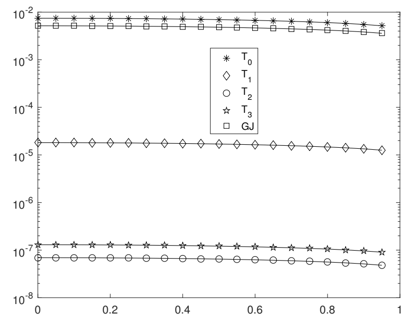

Figure 8: Quadrature errors for Example 6

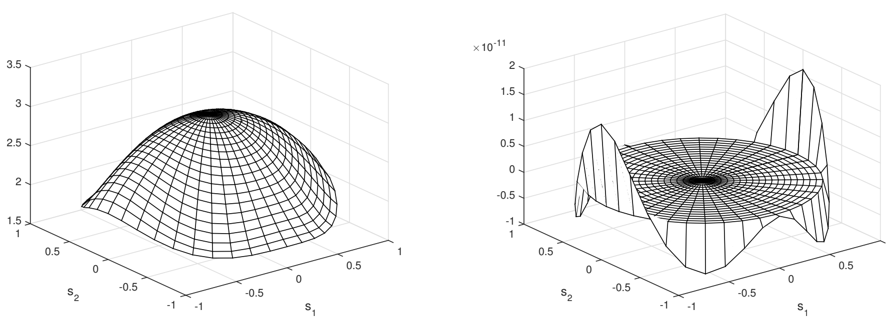

(a) $I\,(f;s)$ (b) Quadrature errors

Figure 9: Integration of (25)-(26) over $\mathbb{B}^2$.

Note again the integrands as shown in (21)-(22), although now the r and θ integrations have been reversed. Note that $\beta\,(r)$ lacks smoothness around $r=2$ because of the $\cos^{-1}$ function, and it is necessary to compensate for this in the numerical integration of the outer r-integration in (27).

Introduce the further transformations of $[0,1]$:

$$T_4(r) = 3r^2 - 2r^3, \tag{28}$$

$$T_5(r) = 10r^3 - 15r^4 + 6r^5. \tag{29}$$

They are the probability density functions of the beta distribution with $B(2,2)$

and $B(3,3)$, respectively. These satisfy

$$\begin{aligned} &T\,(0) = 0, \quad T\,(1) = 1, \\ &T'\,(r) > 0, \qquad 0 < r < 1, \\ &T'\,(0) = T'\,(1) = 0. \end{aligned}$$

The transformation T_5 also has zero second derivatives at 0 and 1, and T_4 and T_5 have a simple extension with even higher derivatives being set to zero. Apply one of these transformations to the outer r-integrals in (27), say with n nodes. This will compensate for the possible ill-behaviour of the integrand when $r \approx 2$.

Example 7 *Consider the integral*

$$I(1;s) \equiv \int_{\mathbb{B}^2} \frac{1}{\mid w - s \mid^{\alpha}} dw$$

where $\alpha = \pi/4$ and $s = (1,0)$. We use the four functions $T_j(r)$, (10)-(11) *and* (28)-(29) *for the r-integration and no transformation is used for the θ-integration. Both the θ-integration and the r-integration are then approximated using Gauss-Legendre quadrature with n nodes for the integral. The true value of the integration is calculated with large n. The column labeled "Ratio" gives the ratio of successive errors. See Table 1.*

	T_1		T_2		T_4		T_5	
n	Error	Ratio	Error	Ratio	Error	Ratio	Error	Ratio
4	2.21e-02	0.00	4.51e-02	0.00	3.09e-03	0.00	5.59e-03	0.00
8	3.15e-03	7.02	5.96e-03	7.59	1.41e-04	21.95	9.61e-06	581.54
16	4.27e-04	7.39	7.90e-04	7.54	5.39e-06	26.10	8.10e-08	118.63
32	5.57e-05	7.66	1.03e-04	7.70	1.98e-07	27.23	5.77e-10	140.32
64	7.12e-06	7.82	1.31e-05	7.83	7.06e-09	28.02	3.91e-12	147.82
128	9.01e-07	7.91	1.66e-06	7.91	2.48e-10	28.49	1.95e-14	199.91
256	1.13e-07	7.95	2.08e-07	7.95	8.63e-12	28.73	3.55e-15	5.50

Table 1: Numerical examples using (27) with various transformations

If (20) is used to calculate the integration, two transformations will be needed, one for the r-integration and one for the θ-integration. Consider the integral

$$\begin{aligned} I(1;s) &\equiv \int_{\mathbb{B}^2} \frac{1}{\mid w - s \mid^{\alpha}} dw \\ &= \int_{-\pi/2}^{\pi/2} \int_0^{2\cos(\theta)} r^{1-\alpha}\, dr\, d\theta = \int_{-\pi/2}^{\pi/2} \frac{(2\cos(\theta))^{2-\alpha}}{2-\alpha}\, d\theta \end{aligned} \tag{30}$$

The integrand $(2\cos(\theta))^{2-\alpha}$ is not smooth around $\pi/2$ and $-\pi/2$ as long as α is not 1. So, it is necessary to compensate for this in the numerical integration of θ-integration.

θ-int	T_0				T_5			
r-int	T_1		T_2		T_1		T_2	
n	Error	Ratio	Error	Ratio	Error	Ratio	Error	Ratio
8	6.62e-04	0.00	1.24e-04	0.00	2.16e-03	0.00	1.62e-03	0.00
16	2.99e-05	22.15	8.76e-06	14.10	2.07e-05	104.13	3.98e-07	4069.07
32	1.27e-06	23.62	4.51e-07	19.43	8.11e-07	25.54	2.99e-09	133.00
64	5.18e-08	24.43	2.18e-08	20.70	3.00e-08	27.04	2.11e-11	141.94
128	2.10e-09	24.64	1.03e-09	21.16	1.07e-09	27.96	1.42e-13	148.37
256	8.59e-11	24.48	4.82e-11	21.35	3.77e-11	28.47	8.88e-16	160.00

Table 2: Numerical examples using (20) with various transformations

Example 8 *This example shows the numerical integration of* (30) *with various transformations for r- and θ-integration. Note that $\alpha = \pi/4$, $s = (1, 0)$, and $T_0(x) = x$. This example shows that choosing a right transformation for the θ-integration will improve the effect of transformations in the r-integration. See Table 2.*

3.3 The case $\alpha = 1$.

Applying the change of variable of (17), the integral

$$I(f; s) = \int_{\mathbb{B}^2} \frac{f(t)}{|t - s|} dt \tag{31}$$

becomes

$$I(f; s) = \int_0^{2\pi} \int_0^{R(\theta)} f(s + r\cos\theta, r\sin\theta)\ dr\, d\theta. \tag{32}$$

This integrand is generally smooth. Thus no transformation of the r-variable is needed to obtain rapid convergence.

3.4 Rotating $\mathbb{B}^2$

For $s \in \mathbb{B}^2$ the disk $\mathbb{B}^2$ is rotated so that the singularity is on the line joining $(0, 0)$ and $(1, 0)$. To carry this out, begin by finding ψ, the angle between the positive x-axis and the radial line through s. Introduce

$$A = \begin{bmatrix} \cos\psi & -\sin\psi \\ \sin\psi & \cos\psi \end{bmatrix}.$$

Then

$$A \begin{bmatrix} |s| \\ 0 \end{bmatrix} = s.$$

In the integral

$$I(g; s) = \int_{\mathbb{B}^2} g(w; s) dw, \qquad s \in \overline{\mathbb{B}}^2,$$

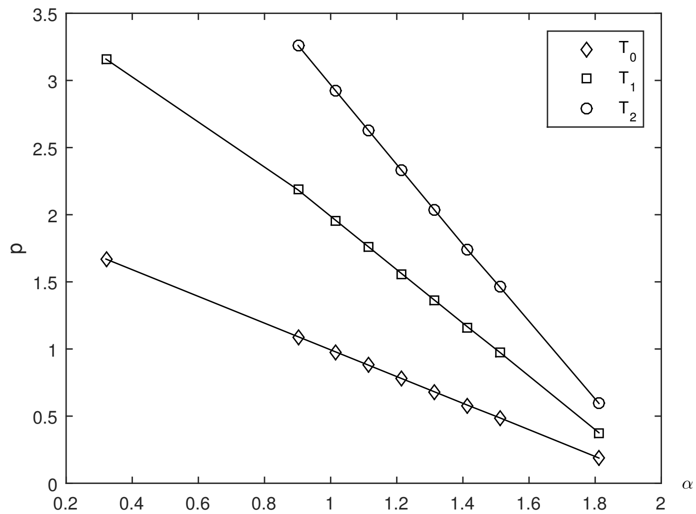

Figure 10: Convergence powers p for (33).

introduce the change of variable $w = At$:

$$I\left(g; s\right) = \int_{\mathbb{B}^2} g(At; s) dt,$$

noting the determinant of the Jacobian of the rotational transformation is 1. In this new integral, the point $\widehat{s} \equiv \left(\left|s\right|, 0\right)^{\mathrm{T}}$ is the singular point in the integration. Of special note for singular integrals of the form (2)-(4),

$$\begin{aligned} \left|s - w\right| &= \left|s - At\right| = \left|A\left(A^{\mathrm{T}} s - t\right)\right| \\ &= \left|A^{\mathrm{T}} s - t\right| = \left|\widehat{s} - t\right|. \end{aligned}$$

3.5 Rates of convergence

To study the rate of convergence of our numerical method (23), the convergence of the errors or that of the successive differences was studied. The error was observed on some interval $[r\cos\theta, r\sin\theta]$, with $0 \le r \le 0.9$. This smaller interval was chosen because (1) the method is different when including a boundary point, and (2) there are difficulties with the numerical method near to the boundary. As a particular case, the rate of convergence was studied for the case of the singularity

$$k\left(\rho\right) = \rho^{-\alpha}, \qquad 0 < \alpha < 2. \tag{33}$$

The integral being transformed is (25) with $f\left(t\right) \equiv 1$.

A sequence of values of $\alpha \in (0, 2)$ was chosen, avoiding special values such as $\alpha = 1$ for which the convergence is more rapid. The error model

$$I - I_N \approx \frac{c}{N^p} \tag{34}$$

was studied, with N the number of quadrature nodes in $\mathbb{B}^2$ and some $p > 0$, to see how well the model fit the computed error. For a given $\alpha \in (0, 2)$, the error was observed for $N = 2^n \times 2^{n+1}, \quad n = 1, 2, \ldots$ This model (34) fit well the errors, although the details are omitted here. Following this, the corresponding p of the assumed relation (34) was determined. Figure 10 shows the empirical results for these powers p with varying α and with the transformations $T_0(r) \equiv r$, T_1, and T_2 defined earlier in (10)-(11). These empirical results show a linear pattern as regards the relationship of α and p, and they lead to the quite good estimates

$$p \approx \begin{cases} 2 - \alpha, & T_0, \\ 4 - 2\alpha, & T_1, \\ 6 - 3\alpha, & T_2. \end{cases} \tag{35}$$

This result is consistent with [9, Exam. 4, p. 599].

3.6 Error behavior near the boundary

Recall that (2)–(3) with the singular point $s = (s_1, 0)$ can be written as

$$I_\alpha(f; s) = \int_0^{2\pi} \int_0^{R(\theta)} f(s_1 + r\cos(\theta), r\sin(\theta)) r^{-\alpha+1} \, dr \, d\theta. \tag{36}$$

If we use the trapezoidal rule for the outside integration over $[0, 2\pi]$, we need to understand how the trapezoidal rule 'behaves' for $R(\theta)$ as s_1 varies between 0 and 1, but $s_1 < 1$, always. This is the topic of the current section. We will assume that f is a smooth function, for example a polynomial, so the main emphasis is on the integration of the kernel function $r^{-\alpha+1}$. Figures 4, 5, and 7 all show an error increase towards the boundary $s_1 = 1$ and this seems to be independent of the method used. At the end of this section we will see how to modify the numerical integration methods to ensure an error smaller than a given bound ε.

In the above integral (36) we can substitute $r = R(\theta)t$ to transform the r-integration to a t–integration over $[0, 1]$ and then use a scaling of the form $t = u^q$, $q \geq 1$, to smooth the behavior of the inner integral at $u = 0$. Doing this leads to

$$\begin{aligned} I_\alpha(f, s) = \int_0^{2\pi} & qR(\theta)^{-\alpha+2} \times \\ & \int_0^1 u^{q(2-\alpha)-1} f(s_1 + R(\theta)u^q \cos(\theta), R(\theta)u^q \sin(\theta)) \, du \, d\theta \end{aligned} \tag{37}$$

By using, for example,

$$q = \frac{3}{2 - \alpha} + 1$$

the exponent of the u will be larger than 2, so the integrand is twice continuously differentiable and a weighted Gaussian quadrature rule will approximate the inner integral

$$\begin{aligned}F_\alpha(s,\theta) &= \int_0^1 u^{q(2-\alpha)-1} f(s_1 + R(\theta)u^q\cos(\theta), R(\theta)u^q\sin(\theta))\,du \\ &\approx \sum_{j=1}^{M} \omega_j^{(M)} f(s_1 + R(\theta)(\xi_j^{(M)})^q\cos(\theta), R(\theta)(\xi_j^{(M)})^q\sin(\theta)) \\ &=: F_{\alpha,M}(s,\theta) \qquad (38)\end{aligned}$$

with a high precision. Here $\omega_j^{(M)}$ and $\xi_j^{(M)}$, $j = 1, \ldots, M$, are weights and nodes of a weighted Gauss quadrature on $[0, 1]$. We will use $M = 20$ in our examples below and assume that we can use $F_\alpha(s, \theta) = F_{\alpha,20}(s, \theta)$. This assumption is verified by error estimates with the help of larger M values.

This leaves us with the integration

$$\begin{aligned}I_\alpha(f,s) &= \int_0^{2\pi} qR(\theta)^{2-\alpha} F_\alpha(s,\theta)\,d\theta \\ &\approx \frac{2\pi q}{N}\sum_{j=0}^{N-1} R\left(\frac{2\pi}{N}j\right)^{2-\alpha} F_{\alpha,M}(s, \frac{2\pi}{N}j) \\ &=: I_{\alpha,M,N}(f,s) \qquad (39)\end{aligned}$$

Again we assume that the main problem for the integration is the term $R(\theta)^{2-\alpha}$ and the function F_α is well behaved. For some applications the function F_α might also have some more complicated behavior, but as long as F_α is smooth, standard error estimations and extrapolation can be applied.

If we look at the function

$$R(\theta) = -s_1\cos\theta + \sqrt{1 - s_1^2\sin^2(\theta)},$$

given in (18), we see that the first term is smooth and the problem for the integration arises from the second term. So we concentrate from now on the following integral

$$J_\beta(s_1) \quad := \quad \int_0^{2\pi} (1 - s_1^2\sin^2(\theta))^{\frac{\beta}{2}}\,d\theta. \qquad (40)$$

where $\beta = 2 - \alpha$, and its numerical integration

$$J_{\beta,N}(s_1) \quad := \quad \frac{2\pi}{N}\sum_{j=0}^{N-1} f_{\beta,s_1}\left(\frac{2\pi}{N}j\right) \qquad (41)$$

$$f_{\beta,s_1}(\theta) \quad := \quad \left(1 - s_1^2\sin^2(\theta)\right)^{\frac{\beta}{2}} \qquad (42)$$

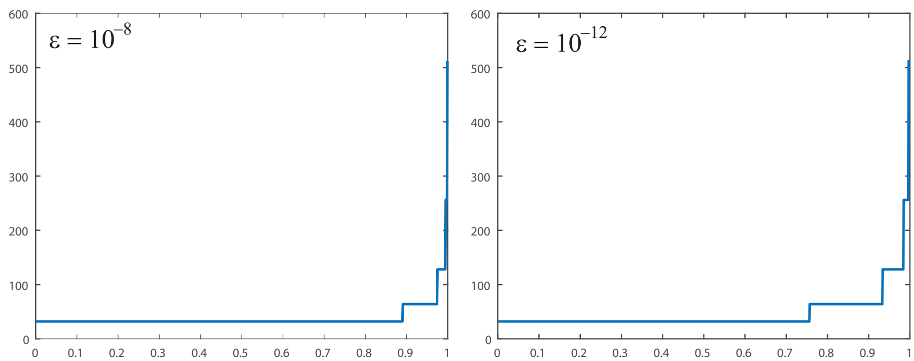

Figure 11: The functions $N = \aleph_{0.5,\varepsilon}(s_1)$, for $\varepsilon = 10^{-8}$ (left), and $\varepsilon = 10^{-12}$ (right), on $s_1 \in [0, 0.999]$

To estimate the error of the trapezoidal rule for f_{β,s_1} we need the Fourier expansion which is given by

$$f_{\beta,s_1}(\theta) \;=\; \sum_{j=0}^{\infty} \binom{\beta/2}{j} (-1)^j s_1^{2j} \sin^{2j}(\theta) \tag{43}$$

$$\;=\; \sum_{k\in\mathbb{Z}} c_{\beta,2k}(s_1) e^{2ki\theta} \tag{44}$$

where

$$c_{\beta,2k}(s_1) \;=\; \left(\frac{s_1}{2}\right)^{2k} \binom{\beta/2}{k} {}_2F_1(-\frac{\beta}{2} + k, k + \frac{1}{2}; 2k+1; s_1^2) \tag{45}$$

with the hypergeometric function ${}_2F_1$, see [1]. The error of the trapezoidal rule is given by

$$E_\beta^N(s_1) \;:=\; |J_\beta(s_1) - J_{\beta,N}(s_1)| \;=\; 2\pi \left| \sum_{j\in\mathbb{Z}\setminus\{0\}} c_{\beta,jN}(s_1) \right| \tag{46}$$

This function allows us to estimate the necessary N to approximate $J_\beta(s_1)$ by $J_{\beta,N}(s_1)$ with an error smaller than a given ε. We will only look for N values that are powers of 2:

$$\aleph_{\beta,\varepsilon}(s_1) \;:=\; \min\{2^j \mid E_\beta^{2^j}(s_1) < \varepsilon, j \geq 5\}$$

Here we used 5, so that at least 32 points are used for the trapezoidal rule. This might be too large for certain smooth functions and will need to be adjusted for more complicated functions. In Figure 11 we plot two $\aleph$ functions for $\beta = 1/2$, so $\alpha = 1.5$, and $\varepsilon = 10^{-8}$, 10^{-12}. We see that for a large range of s_1 values $N = 32$ is sufficient to guarantee a small error in evaluating the single integral

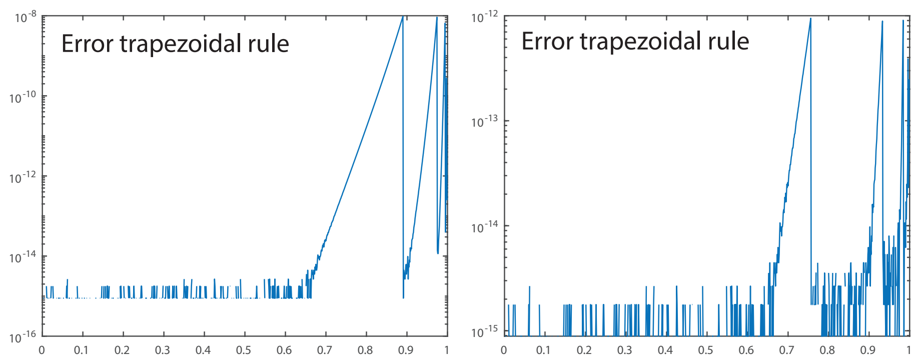

Figure 12: The error of the trapezoidal rule $J_{\beta,\aleph_{0.5,\varepsilon}(s_1)}(s_1)$ for $\varepsilon = 10^{-8}$ (left), and $\varepsilon = 10^{-12}$ (right), on $s_1 \in [0, 0.999]$

(40). Close to the right endpoint $s_1 \approx 1$ we will need to increase the N value. If we use the calculated $N = \aleph_{2-\alpha,\varepsilon}(s_1)$ values for the calculation of $J_{\beta,N}(s_1)$ and plot the error we get the graphs in Figure 12. Figure 12 shows that by using the N values, given by $\aleph_{\beta,\varepsilon}$, the error of the one dimensional integrals are well controlled and below the required maximum. We like to emphasize that for the generation of the error graphs in Figure 12 we use 1000 values for s_1, $s_1 = j/1000$, $j = 0, \ldots, 999$. So Figure 12 and the following Figures 13 and 14 show the error up to points extremely close to the boundary of the domain.

Now we put the two numerical methods together for the approximation of $I_\alpha(f, s)$, see (37). We use $F_{\alpha,20}(s, \theta)$, see (38), and N given by $\aleph_{\beta,\varepsilon}$ for the calculation of $I_{\alpha,20,N}(f, s)$, see (39).

We use the following approximation

$$\begin{aligned} I_\alpha(f,s) &= \int_0^{2\pi} qR(\theta)^{2-\alpha} F_\alpha(s,\theta)\, d\theta \\ &\approx \frac{2\pi q}{N} \sum_{j=0}^{N-1} R\left(\theta_{N,j}\right)^{2-\alpha} \times \\ &\qquad \sum_{j=1}^{M} \omega_j^{(M)} f(s_1 + R(\theta_{N,j})(\xi_j^{(M)})^q \cos(\theta_{N,j}), R(\theta)(\xi_j^{(M)})^q \sin(\theta_{N,j}) \\ &=: I_{\alpha,\varepsilon,M}(f,s), \text{ where } \theta_{N,j} = \frac{2\pi}{N} j,\ N = \aleph_{2-\alpha,\varepsilon}(s_1) \end{aligned} \tag{47}$$

where $\varepsilon > 0$ is a predetermined level of precision.

To minimize the impact of a complicated function f, we use the simple functions $f_0(s) = 1$ and $f_1(s_1, s_2) = e^{s_1 s_2}$. To estimate the error we calculate

$$I_{\alpha,\varepsilon,20}(f,s) - \widetilde{I}_{\alpha,\varepsilon,40}(f,s).$$

The difference between I and $\widetilde{I}$ is that we use $N = 4\aleph_{2-\alpha,\varepsilon}(s_1)$ instead of

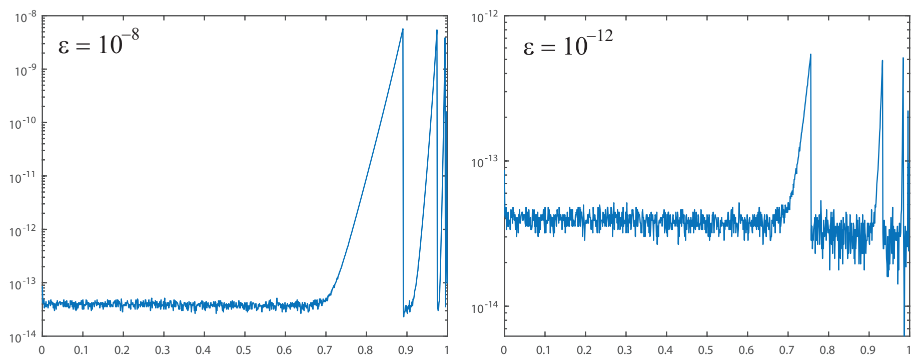

Figure 13: The error of $I_{1.5,\varepsilon,20}(f_0, s_1)$ with $\varepsilon = 10^{-8}$ (left), and $\varepsilon = 10^{-12}$ (right), on $s_1 \in [0, 0.999]$

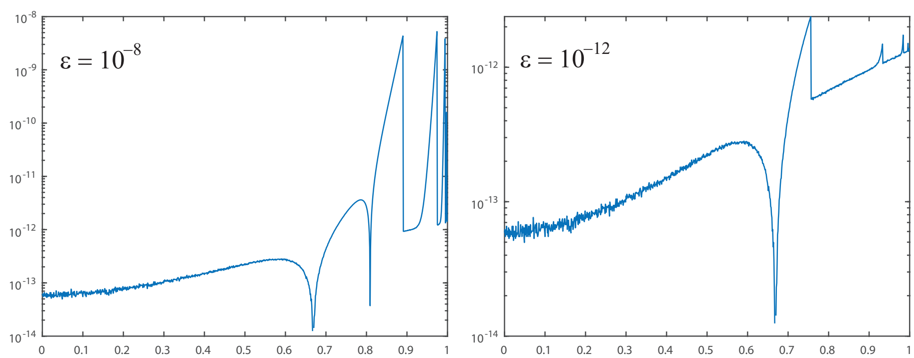

Figure 14: The error of $I_{1.5,\varepsilon,20}(f_1, s_1)$ with $\varepsilon = 10^{-8}$ (left), and $\varepsilon = 10^{-12}$ (right), on $s_1 \in [0, 0.999]$

$N = \aleph_{2-\alpha,\varepsilon}(s_1)$ for the calculation of $\widetilde{I}$. Figures 13 and 14 show the errors of $I_{1.5,\varepsilon,20}(f, s)$, $\varepsilon = 10^{-8}, 10^{-12}$ for f_0 and f_1.

As we expect the estimated values for N work better in the case of the simpler function $f_0(s)$, but the slightly more complicated function $f_1(s)$ still shows errors that are mostly smaller than the given ε. So the function $\aleph_{\beta,\varepsilon}$, $\beta = 2 - \alpha$, is a good starting point for finding sufficiently large N values and maybe one additional N value for an error estimation will be sufficient to adjust the N to keep the error below a given bound. Figures (13) and (14) both show that we are able to control the quadrature error up to the boundary by using the estimated values for N.

4 Transforming other planar regions

Assume the existence of an explicitly known continuously differentiable mapping

$$\Phi : \overline{\mathbb{B}}^2 \underset{onto}{\xrightarrow{1-1}} \overline{\Omega} \tag{48}$$

with Ω a simply connected region in the plane. Let

$$J(t) \equiv (D\Phi)(t) = \left[\frac{\partial \Phi_i(t)}{\partial t_j}\right]_{i,j=1}^{2}, \qquad t \in \overline{\mathbb{B}}^2$$

denote the Jacobian matrix of the transformation. Assume $J(t)$ satisfies

$$\det J(t) \neq 0,$$

except possibly on a set of measure zero. See [5] for a discussion of methods for creating such mappings Φ.

Consider the integral

$$I(f, \sigma) = \int_{\Omega} f(\tau; \sigma)\, d\tau, \quad \sigma \in \Omega,$$

with σ denoting a point singularity in the integrand. Let $\tau = \Phi(t)$, $t \in \mathbb{B}^2$. Then

$$I(f, \Phi(s)) = \int_{\mathbb{B}^2} f(\Phi(t); \Phi(s))\, |\det J(t)|\, dt, \quad \sigma = \Phi(s), \quad s \in \mathbb{B}^2. \tag{49}$$

We illustrate using this with an elliptical region,

$$\Phi(\tau_1, \tau_2) = (a\tau_1, b\tau_2). \qquad \tau \in \mathbb{B}^2, \tag{50}$$

with $a, b > 0$. Let $\sigma = \Phi(s)$ for some $s \in \mathbb{B}^2$. Then $\det J(t) \equiv ab$, and

$$I(f, \Phi(s)) = ab \int_{\mathbb{B}^2} f(\Phi(\tau); \Phi(s))\, d\tau. \tag{51}$$

The earlier quadrature methods can now be applied to this integral.

Example 9 *Evaluate*

$$I(f; \sigma) = \int_{\Omega} \frac{f(\tau)}{|\tau - \sigma|^{\alpha}} d\tau \tag{52}$$

with Ω the ellipse of (50) and $\sigma \in \Omega$, using the transformed integral (51). We show graphs of the case with $(a, b) = (0.75, 2.0)$, $\alpha = 1.5$, $n = 32$,

$$f(\tau) \equiv f(x, y) = \cos\left(x(y+1) + 2y^2\right). \tag{53}$$

The number of nodes is 32×64, $n = 32$. The integration transformation is T_1, given in (10), and the boundary formulation (20) is used with $4n$ nodes in the radial direction and $8n$ in the angular direction. The integral is shown in Figure 15(a), and the error is shown in Figure 15(b). The largest error is along the boundary.

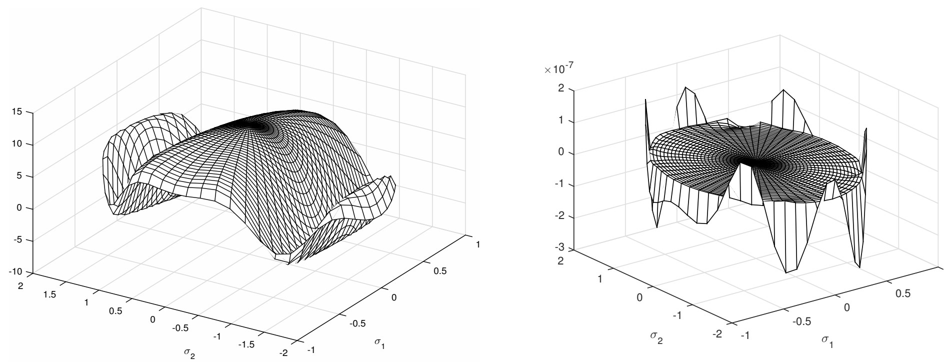

(a) The integral $I\left(f;\sigma\right)$ (b) The error

Figure 15: Integration of (52)-(53) over an ellipse with $n = 32$.

5 Smoothing a singularity in $\mathbb{B}^3$

Consider approximating

$$I(f;v) = \int_{\mathbb{B}^3} f(t)k(|v-t|)\,dt \tag{54}$$

For simplicity, assume $v = (0,0,s)$ with $0 \le s < 1$. Use the change of variables

$$t = (0,0,s) + \rho\left(\cos\varphi\sin\theta, \sin\varphi\sin\theta, \cos\theta\right) \tag{55}$$

with $0 \le \varphi \le 2\pi$, $0 \le \theta \le \pi$. To find the limits for ρ, solve $|t| = 1$:

$$\begin{aligned} \rho^2\sin^2\theta + (s+\rho\cos\theta)^2 &= 1, \\ \rho^2 + 2s\rho\cos\theta - \left(1-s^2\right) &= 0. \end{aligned}$$

The desired positive root is

$$\begin{aligned} \mathrm{P}_\theta &= -s\cos\theta + \sqrt{s^2\cos^2\theta + 1 - s^2} \\ &= -s\cos\theta + \sqrt{1 - s^2\sin^2\theta}, \end{aligned} \tag{56}$$

just as earlier in (18). The integral $I(f;v)$ transforms to

$$I(f;v) = \int_0^{2\pi}\int_0^{\pi}\sin\theta\int_0^{\mathrm{P}_\theta}\rho^2 f\left(t\right)k\left(\rho\right)\,d\rho\,d\theta\,d\varphi \tag{57}$$

with t given by (55). Perform the ρ-integration, and introduce

$$\begin{aligned} \gamma\left(\chi\right) &\equiv \int_0^{\mathrm{P}_\theta}\rho^2 f\left(t\right)k\left(\rho\right)\,d\rho, \\ \chi &= \left(\cos\varphi\sin\theta, \sin\varphi\sin\theta, \cos\theta\right) \in \mathbb{S}^2. \end{aligned} \tag{58}$$

Then

$$I(f;v) = \int_{\mathbb{S}^2} \gamma(\chi)\, d\chi$$

The function $\gamma(\chi)$ is approximated as in the planar case. A transformation T is used, as before in (23), followed by Gauss-Legendre quadrature. Approximate $\gamma(\chi)$ as in the unit disk case. Then approximate $I(f;v)$ using spherical integration. A variety of such methods are discussed in [6, Chap. 5], [13, §2.7]. We use the product method given in [6, (5.2)].It uses $2n^2$ nodes, n nodes for the θ-integration and $2n$ nodes for the φ-integration; and it has degree of precision $2n-1$. The total number of nodes is $n \times 2n^2$.

As the remaining case, let $v = (0,0,1)$. Modifying (55), let

$$t = (0,0,1) - \rho(\cos\varphi\sin\theta, \sin\varphi\sin\theta, \cos\theta) \tag{59}$$

for $0 \le \varphi \le 2\pi$. Solve for $|t| = 1$. This leads to

$$\mathrm{P}_\theta = 2\cos\theta.$$

Then

$$t = (0,0,1) - \rho(\cos\varphi\sin\theta, \sin\varphi\sin\theta, \cos\theta),$$

for $0 \le \theta \le \frac{1}{2}\pi$, $0 \le \rho \le \mathrm{P}_\theta$, $0 \le \varphi \le 2\pi$. The integral to be evaluated is

$$I(f) = \int_0^{\pi/2} \sin\theta \int_0^{2\pi} \int_0^{\mathrm{P}_\theta} \rho^2 f(t)\, k(\rho)\, d\rho\, d\varphi\, d\theta. \tag{60}$$

Gauss-Legendre quadrature with n nodes is used for $0 \le \theta \le \frac{1}{2}\pi$, and the trapezoidal rule with $2n$ nodes is used for $0 \le \varphi \le 2\pi$. The total number of nodes is $n \times 2n^2$.

Example 10 *Consider the integral*

$$I(1;v) = \int_{\mathbb{B}^3} \frac{1}{|v-u|^\alpha}\, du, \qquad v \in \mathbb{B}^3, \tag{61}$$

with $0 < \alpha < 3$, which can be evaluated explicitly. Letting $\alpha = 2/\pi$, Figure 16 shows the result of using the identity transformation ($T_0(\rho) = \rho$), a simple quadratic transformation ($T_1(\rho) = \rho^2$), and the cubic transformation ($T_2(\rho) = \rho^3$). This calculation used $n = 16$, except with the boundary point $v = (0,0,1)$ where $n = 32$ was used. When using the transformations T_1 and T_2, there is a problem near to and on the boundary. As earlier, using a larger value for n when near to the boundary will improve the error.

5.1 Rotating $\mathbb{B}^3$

For the singular point v of (54) not located on the line segment joining $(0,0,0)$ and $(0,0,1)$, the ball can be reflected to move the singular point to that line segment. Let A denote the Householder matrix satisfying

$$Av = [0,0,|v|]^T.$$

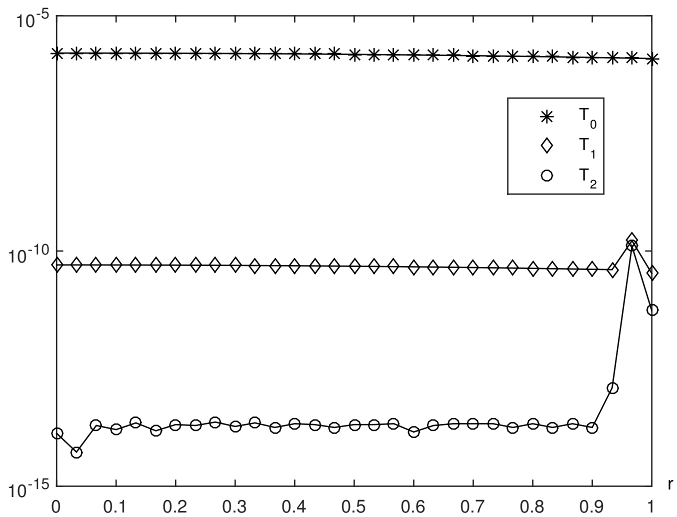

Figure 16: Comparison of errors for (61) using T_0, T_1 and T_2 with $\alpha = 2/\pi$ and $n = 16$.

Recall that A is symmetric and orthogonal. In the integral (54), make the substitution $t = A\tau$:

$$I(f;v) = \int_{\mathbb{B}^3} f(A\tau)\, k(|v - A\tau|) \;\; dt \tag{62}$$

noting that the Jacobian of the transformation has an absolute value of 1 for its determinant. Using

$$\begin{aligned} |v - A\tau| &= |A(Av - \tau)| \\ &= \left| [0, 0, |v|]^T - \tau \right|, \end{aligned}$$

reduces (62) to the earlier case with a singular point between $(0,0,0)$ and $(0,0,1)$

Example 11 *Consider the integral*

$$\begin{aligned} I(f;v) &= \int_{\mathbb{B}^3} \frac{f(u)}{|v-u|^\alpha}\, du, \qquad v \in \mathbb{B}^3, \\ f(u) &= \cos\left(\frac{5u_1^2}{4+u_2} + u_3\right), \end{aligned} \tag{63}$$

with $\alpha = 5/\pi$. We evaluate the integral along the line joining the origin and the boundary point $v = \left(\frac{1}{2\sqrt{2}}, \frac{\sqrt{3}}{2\sqrt{2}}, \frac{1}{\sqrt{2}}\right)$, corresponding to $(\varphi, \theta) = (\pi/3, \pi/4)$.

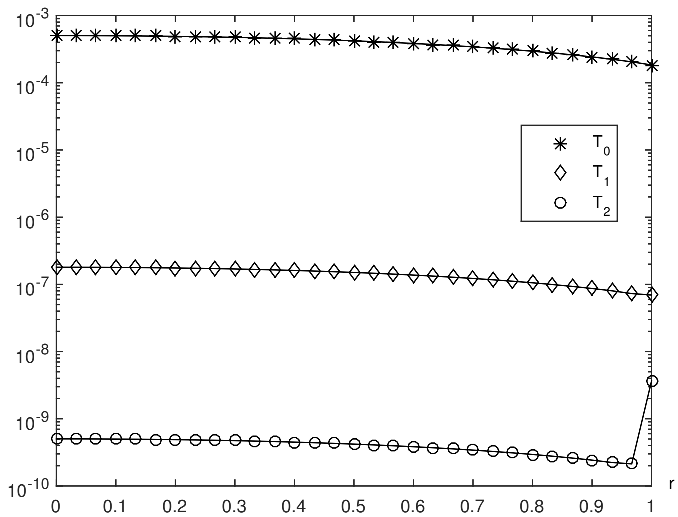

Figure 17: Error for (63) along the line with $\theta = \pi/3$, $\varphi = \pi/4$, with $\alpha = 5/\pi$ and $n = 16$.

The quadrature uses $n = 16$*, except* $n = 32$ *for the boundary point. Figure 17 contains comparisons for the transformations* T_0*,* T_1*, and* T_2*. The option* T_2 *is the better one.*

Example 12 *To have a broader look at the behaviour of the numerical method applied to (61), we observe the error when evaluating over a disk region in* $\mathbb{B}^3$*, obtained by intersecting a plane with* $\mathbb{B}^3$ *and having it pass through the origin. Figure 18(a) contains the disk for our example, with the disk orthogonal to the vector* $d = \left(\frac{\sqrt{3}}{2\sqrt{2}}, \frac{1}{2\sqrt{2}}, \frac{1}{\sqrt{2}}\right)$*, corresponding to* $\varphi = \pi/6$*,* $\theta = \pi/4$*, shown in red. The horizontal disk is the usual* $\mathbb{B}^2$*, the planar unit disk. The exponent* $\alpha = 2/\pi$ *in the integral (61). Figure 18(b) shows the computed value of the integral (61). The error is a function of only* r*, the distance from the origin, and it follows closely what is shown in Figure 16. Again,* $n = 16$ *is used for the quadrature, and* T_2 *is the transformation being used.*

Example 13 *An analogous calculation is done for the integral (63). The quadrature parameter is* $n = 8$*, and it is evaluated over the same disk as in Figure 18(a). The exponent* $\alpha = 4/\pi$ *in the integral (63). Figure 19(a) shows the integral over that disk, and Figure 19(b) shows its error. The maximum error over that disk is* $7.48E - 5$*.*

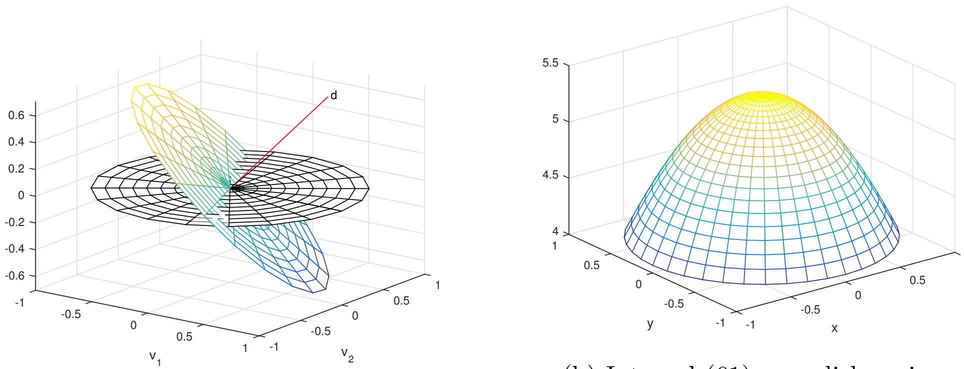

(a) Disk region in $\mathbb{B}^3$, orthogonal to d.

(b) Integral (61) over disk region orthogonal to d.

Figure 18: Integration of (61) over disk region.

5.2 The cases $\alpha = 1, 2$

Consider the kernel $k(\rho) = \rho^{-\alpha}$. In the cases of $\alpha = 1, 2$, the kernel in (57) will have a smooth integrand. Therefore the integrand will be smooth and no smoothing transformation $T(\rho)$ is necessary. The Gauss-Legendre quadrature for the radial integral will work well, as will the trapezoidal rule for the angular integration. The case $\alpha = 1$ occurs frequently in practice. The integral

$$I\left(\frac{-f}{4\pi}; v\right) = \frac{-1}{4\pi} \int_{\mathbb{B}^3} \frac{f(u)}{|v-u|}\, du$$

is called a *Newtonian potential*; it satisfies Poisson's equation,

$$\Delta w = f.$$

See [2] where these quadrature ideas can be applied.

Concluding remarks.

We have presented and illustrated numerical methods for integrals with a point singularity, for integration regions that are diffeomorphic to the unit disk or the unit ball. We thank the reviewers, including the suggestion for using Gauss-Jacobi quadrature.

References

[1] G. Andrews, R.A. Askey, R. Roy, *Special Functions*, Cambridge University Press, 1999.

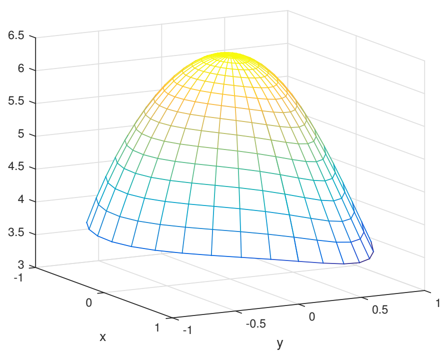

(a) Integral (63) over a disk region.

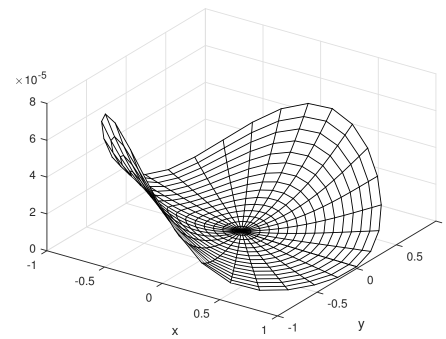

(b) Error in integral (63) over a disk region.

Figure 19: Integration of (63) over disk region.

[2] K. Atkinson. The numerical evaluation of particular solutions for Poisson's equation, *IMA Journal of Numerical Analysis,* **5** (1985), 319-338.

[3] K. Atkinson. *An Introduction to Numerical Analysis*, 2^{nd} ed., John Wiley & Sons, 1989.

[4] K. Atkinson. Quadrature of singular integrands over surfaces, *Electronic Transactions on Numerical Analysis* **17** (2004), pp.133-150.

[5] K. Atkinson, and O. Hansen. Creating domain mappings, *Electronic Transactions on Numerical Analysis* **39** (2012), pp. 202-230.

[6] K. Atkinson and W. Han. *Spherical Harmonics and Approximations on the Unit Sphere : An Introduction,* Lecture Notes in Mathematics #2044, Springer-Verlag, New York, 2012.

[7] M. Botha. A family of augmented Duffy transformations for near-singularity cancellation quadrature, *IEEE Transactions on Antennas and Propagation* **61** (2013), pp. 3123-3134.

[8] A. Chernov and C. Schwab. Exponential convergence of Gauss-Jacobi quadratures for singular integrals over simplices in arbitrary dimension, *SIAM J. Num. Anal.* **50** (2012), pp. 1433-1455.

[9] J. Donaldson and and D. Elliott. A unified approach to quadrature rules with asymptotic estimates of their remainders, *SIAM J. Num. Anal.* **9** (1972), pp. 573-602.

[10] A. Klöckner, A. Barnett, and L. Greengard. Quadrature by expansion: A new method for the evaluation of layer potentials, *Journal of Computational Physics* **252** (2013), pp. 332-349.

[11] J. N. Lyness. An error functional expansion for n-dimensional quadrature with an integrand function singular at a point. *Mathematics of Computation,* **30** (1976), pp. 1-23.

[12] J. Strain. Locally corrected multidimensional quadrature rules for singular functions. *SIAM J. Sci. Comput.* **16** (1995), pp. 992-1017.

[13] A. Stroud. *Approximate Calculation of Multiple Integrals,* Prentice-Hall, Inc., Englewood Cliffs, N.J., 1971.

[14] A.-K. Tornberg. Multi-dimensional quadrature of singular and discontinuous functions. *BIT*, **42** (2002), pp. 644-669.